

# Decimeter Ranging with Channel State Information

Navid Tadayon, *Member, IEEE*, Muhammed T. Rahman, Shuo Han, Shahrokh Valaee, *Senior Member, IEEE*, and Wei Yu, *Fellow, IEEE*

**Abstract**—This paper aims at the problem of time-of-flight (ToF) estimation using channel state information (CSI) obtainable from commercialized MIMO-OFDM WLAN receivers. It was often claimed that the CSI phase is contaminated with errors of known and unknown natures rendering ToF-based positioning difficult. To search for an answer, we take a bottom-up approach by first understanding CSI, its constituent building blocks, and the sources of error that contaminate it. We then model these effects mathematically. The correctness of these models is corroborated based on the CSI collected in extensive measurement campaign including radiated, conducted and chamber tests. Knowing the nature of contaminations in CSI phase and amplitude, we proceed with introducing pre-processing methods to clean CSI from those errors and make it usable for range estimation. To check the validity of proposed algorithms, the MUSIC super-resolution algorithm is applied to post-processed CSI to perform range estimates. Results substantiate that median accuracy of 0.6m, 0.8m, and 0.9m is achievable in highly multipath line-of-sight environment where transmitter and receiver are 5m, 10m, and 15m apart.

**Index Terms**—Indoor positioning, MIMO, OFDM, CSI, Calibration.

## I. INTRODUCTION

ONE of the fundamental challenges of today’s networks is precise estimation of indoor users’ locations. The location of a user is a source of information that can be leveraged to unlock huge technological, social, and business potentials. This is in particular the case for indoor environment, where the signal of the global navigation satellite system (GNSS) is unavailable.

Due to its pervasive deployment and cost-effective nature, positioning using wireless local area networks (WLANs) signals has been at the focus of research for almost a decade. In fact, experimental works have proven that WiFi signals can be used to obtain excellent location accuracy even in harsh multipath environments [1]–[11]. For a comprehensive survey on the success of WiFi in localizing indoor users refer to [12], [13]. This has been a significant advancement as, until recently, ultra-wide-band (UWB) radio was deemed as the only viable solution to get accurate location information [14].

Indoor positioning using WiFi began with power-based ranging using received signal strength (RSS) [8]–[11], [15], [16]. Unfortunately, accurate range estimation with RSS is impossible because: (i) time-domain OFDM signals are highly fluctuating (ii) the amplitude of a signal is directly affected by small-scale fading (iii) signal amplification at the receiver

is controlled by the automatic gain controller (AGC) whose behaviour dynamically varies with channel conditions.

This paper is motivated by the availability of channel-state information (CSI) from Intel [17] and Atheros [18] WiFi chipsets that have enabled CSI to be used for positioning. CSI is a more stable and informative representation of the wireless channel (compared to RSS) between two communicating endpoints. Therefore, it can be used to perform range (time-based or power-based) and angle-of-arrival estimation. When it comes down to implementation, while CSI-based localization with AoA achieved promising outcomes [2]–[4], [19], using CSI to estimate time-of-flight (ToF) measurement has either not been pursued or led to inconsistent results [2]. To our knowledge, the studies that do consider phase-based ranging all use software-defined radio (SDR), an open-source and fine-tuned platform that is expensive to acquire and so is unscalable. On the other hand, our work is based on using commercial off-the-shelf MIMO-OFDM network interface cards (NIC), which are used in laptops and computers, to estimate the range from phase of the CSI. As ToF measurement is crucial to ranging, and subsequently positioning, this raises the question, “What makes ToF estimation using CSI a challenging task?” This paper aims to find an answer to this question. Our goal is multifaceted: First, we aim to discuss some of the often neglected practical issues about CSI and ToF estimation using the CSI. In that vein, we dissect CSI that is obtainable from WiFi chipsets to understand its constituent building blocks, different forms it takes, and the sources of error that contaminate it. We proceed with introducing pre-processing methods to clean CSI from those errors and make it usable for ToF estimation. We then apply the classic super-resolution spectral MUSIC algorithm to the post-processed CSI to obtain accurate and stable range estimates. To our knowledge, this is an achievement that has never been accomplished before.

The inherent appeal of MUSIC algorithm is due to the fact that estimator’s resolvability power is not only determined by the signal bandwidth but also the total signal-to-noise ratio (SNR). More importantly, MUSIC is an efficient and consistent estimator when certain criteria are met.

In doing so, different ideas are examined, including covariance hardening methods, such as spectral smoothing and forward-backward smoothing, and decision fusion algorithms. We demonstrate that decimetre ranging with only 20MHz of spectrum is possible if CSI is properly post-processed and range estimates are intuitively combined.

**Problem Statement:** A holistic view of the problem addressed in this paper is presented in Fig. 1a where the link between a transmitter and receiver is shown: Whereas coherent decoding of data symbols in communications systems requires the knowledge of end-to-end degradation imposed

This research is supported by the Natural Sciences and Engineering Research Council (NSERC).

Authors are affiliated with the University of Toronto (UofT), Toronto, Canada; Email: {tadayon@utoronto.ca, {mt.rahman, shuo.han}@mail.utoronto.ca, and {valaee, weiyu}@ece.utoronto.ca.

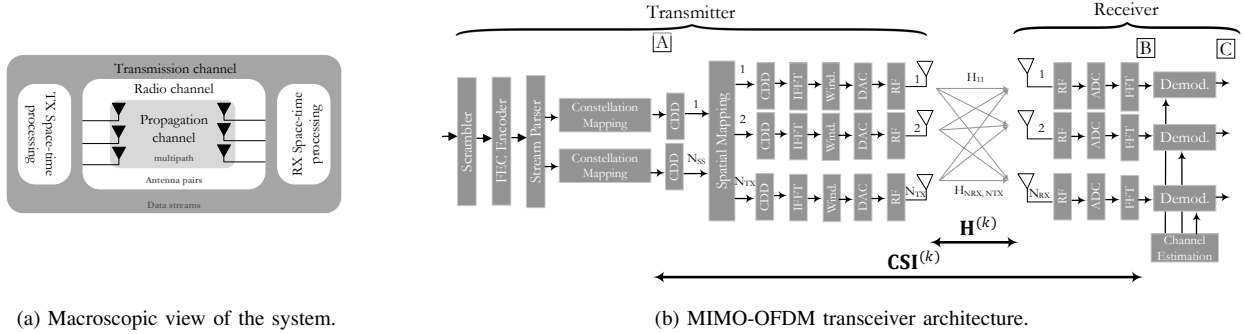


Fig. 1: (left) Depiction of different channels observed at different points along the transceiver chain (right) End-to-end MIMO-OFDM transceiver architecture. Channel from point A to C is the equivalent transmission channel.

between a transmitter’s baseband (BB) and receiver’s BB (named *transmission channel*), location estimation hinges on the knowledge of the channel immediately between the two antennas (named *propagation channel*). Not only these two channels are not the same, but quantifying one from the other is a non-trivial task. The difference between transmission channel  $\mathbf{M}_X$  CSI and propagation channel  $\mathbf{H}$  arises because of (i) lack of synchronization between transmitter/receiver in passband (PB) and (ii) deterministic signal processing operations in transmitter’s BB. In the latter case, cyclic delay diversity (CDD), spatial mapping matrix (SMM), and time-windowing, whose effects are generally incorporated into the CSI matrix, make the receiver believe that the transmitter is several tens of meters away and that the channel is more reflective than it really is.

**Contribution:** In tackling the aforementioned problem, this paper’s contributions are as follows:

- To dissect different deterministic and random phenomena happening in the transmitter and receiver hardware causing  $\mathbf{H}$  and  $\mathbf{CSI}$  to be different.
- To establish the right model for CSI and its relation with the channel matrix.
- To develop pre-processing techniques to eliminate random phases introduced by the insufficiency of synchronization between the transmitter and the receiver.
- To obtain accurate range estimates by applying super-resolution algorithm to the calibrated CSI.

**Organization:** This paper is organized as follows: In Section II, we go over the basics of multiple-input multiple-output orthogonal frequency division multiplexing (MIMO-OFDM) WLAN systems, including their transceiver architecture, channel-sounding, etc. In Section III we show why ToF estimation with CSI is a challenging task, and explain different random and deterministic sources of error contributing to this problem. With the knowledge gained, we tackle the problem of cleaning and calibrating CSI in Section IV. Finally, in Section V, we introduce ideas to obtain more accurate range estimates from the post-processed CSI.

**Notation:** The following notation is adopted throughout this paper:  $a$  (lowercase/regular)  $\rightarrow$  a scalar,  $\mathbf{a}$  (lowercase/boldface)  $\rightarrow$  a vector,  $\mathbf{A}$  (uppercase/boldface)  $\rightarrow$  a matrix. For matrix  $\mathbf{A}$ ,  $a_{r,q}$  is its  $(r, q)$ th element,  $\mathbf{A}^T$  is its

transpose,  $\mathbf{A}^*$  is its conjugate, and  $\mathbf{A}^H$  is its Hermitian.

## II. BACKGROUND

### A. Channel State Information (CSI)

Without properly compensating for the propagation and asynchronization effects, the receiver has no way of detecting what was transmitted. To that end, and through a mechanism named *channel sounding*, the receiver obtains an estimate of wireless channel. This is accomplished by sending a training sequence that is known to both transmitter and receiver. For a wideband MIMO-OFDM system, the estimate of the channel is a collection of complex matrices one for each OFDM subcarrier. It is such information that is universally known as channel state information (CSI). Once CSI is known, it is used by the equalizer in order to cancel out any deterioration (e.g. phase shift, attenuation, etc.) that was imposed on the transmitted data. For packet-based MIMO-OFDM IEEE802.11(n) systems, training sequences, namely high throughput long training fields (HT-LTF), are sent in the preamble, which is instantly used by the receiver to derive CSI.

### B. WLAN Transceiver Architecture

Fig. 1b shows the general structure of the MIMO-OFDM WLAN transmitter. An encoded high-rate bit stream is fed to the stream parser to create  $N_{ss}$  spatial streams. These spatial streams are modulated using constellation mappers (e.g. QAM) to create stream of symbols. As explained before, the transmitter may only send  $N_{ss} \leq \text{rank}(\mathbf{H})$  parallel streams, where  $\mathbf{H}$  is the true channel matrix, and violating this rule would result in loss of data. Note that  $\text{rank}(\mathbf{H}) \leq \min(N_{tx}, N_{rx})$  (with the equality holding when the channel is rich scattering), where  $N_{tx}$ ,  $N_{rx}$  are the number of transmit and receive antennas, respectively.

Next, spatial streams are cyclically shifted through a mechanism named cyclic delay diversity (CDD) to create extra frequency diversity and make sure no unintended beamforming takes place when sending common information (e.g. headers) from all transmit antennas.

The spatial mapping maps fewer number of spatial streams to larger number of transmit antennas [20]. This is especially crucial in situations where lower number of streams is to be

carried by larger number of transmit chains. The existence of CDD and spatial mapping matrix are among the main reasons to render one-way measurements of time-of-flight (ToF) for ranging difficult. Moving forward, a second CDD layer is applied to each transmit chain and frequency domain samples are fed to inverse fast Fourier transform (IFFT) to create time-domain samples. These samples are then simultaneously sent from all transmit chains.

Referring to Fig. 1, the receiver output  $\mathbf{y}$  at point “B”, is related to transmitter input  $\mathbf{x}$  at point “A” through the following matrix equation:

$$\mathbf{y}^{(k)} = \begin{bmatrix} \mathbf{H}^{(k)} \end{bmatrix}_{N_{\text{rx}} \times N_{\text{tx}}} \cdot \begin{bmatrix} \Phi_{\mathbf{a}}^{(k)} \end{bmatrix}_{N_{\text{tx}} \times N_{\text{tx}}} \cdot \begin{bmatrix} \mathbf{Q}^{(k)} \end{bmatrix}_{N_{\text{tx}} \times N_{\text{ss}}} \cdot \begin{bmatrix} \Phi_{\mathbf{b}}^{(k)} \end{bmatrix}_{N_{\text{ss}} \times N_{\text{ss}}} \cdot \mathbf{x}^{(k)} \quad (1)$$

where  $\mathbf{H}^{(k)}$ ,  $\mathbf{Q}^{(k)}$ ,  $\Phi_{\mathbf{a}}^{(k)}$  and  $\Phi_{\mathbf{b}}^{(k)}$  are, respectively, the channel matrix, the spatial mapping matrix, and the first, and the second CDD matrices at the  $k$ th subcarriers,  $k = 1, \dots, N_{\text{nz}}$ , where  $N_{\text{nz}}$  is the number of (non-zero) subcarriers within the band of interest out of the total of  $N_{\text{sc}}$  subcarriers (e.g.  $N_{\text{nz}} = 56$  and  $N_{\text{sc}} = 64$  for  $B = 20\text{MHz}$  in IEEE 802.11n systems). More details on the composition of  $\mathbf{Q}^{(k)}$ ,  $\Phi_{\mathbf{a}}^{(k)}$ , and  $\Phi_{\mathbf{b}}^{(k)}$  are provided in the next sub-section.

1) *Cyclic Delay Diversity (CDD)*: Despite that the payload part of a packet is destined only to a given destination, the packet preamble is meant to be heard/decoded by everyone. To ensure that the header is received by all, and to avoid inadvertent beamforming across the antennas, CDD is used [21]. This is achieved by sending the same header OFDM symbols over different antennas while cyclically shifting them so that (i) all RF chains are utilized, thus, longer communication range is obtained (ii) no unintended beamforming is experienced. The effect of CDD on transmitting common header information changes the multipath nature of the channel as seen by the receiver. To simplify the transceiver architecture, CDD is always applied no matter which portion of packet is being sent, header or payload. The choice of CDD is implementation dependent. We observe that at times, even the same access point (AP) will use different CDD values for the same number of streams. Nonetheless, the standard [22] puts forth some recommendations. Ranging with the raw CSI obtained from the NIC (without accounting for CDDs) may give rise to an accuracy that is off by several tens of meters.<sup>1</sup>

2) *Spatial Mapping Matrix (SMM)*: The spatial mapping operation is the most crucial component of MIMO-OFDM systems assuming tasks such as transmit beamforming, spatial multiplexing, spatial diversity, and so on. This is often implemented through linear matrix operation  $\mathbf{Q}^{(k)}$  as shown in (1) and is an implementation-dependent matter. If  $N_{\text{ss}} = N_{\text{tx}}$ , often direct mapping takes place, i.e.  $\mathbf{Q}^{(k)} = \mathbf{I}$ , where  $\mathbf{I}$  is the identity matrix. However, when  $N_{\text{ss}} < N_{\text{tx}}$ , indirect mapping may be adopted [20]. In the latter case, the effect of SMM is similar to having more echoes than those added by the

propagation environment. For this reason, imposition of SMM has similar effect as having *virtual* echoes.

### C. Channel Sounding

Channel sounding is the mechanism of obtaining CSI at the receiver. This is done by transmitting known HT-LTF sequences. HT-LTF sent over  $j_{\text{ss}}$ th stream is a unique sequence  $\mathbf{x}_{j_{\text{ss}}} = (x_{j_{\text{ss}}}^{(k)}, k = 1 \dots N_{\text{sc}})$  where  $x_{j_{\text{ss}}}^{(k)} \in \{-1, 1\}$ . To probe a single dimension of the multi-dimensional (MIMO) channel, one  $\mathbf{x}_{j_{\text{ss}}}$  is sent on each spatial stream, for the total of  $N_{\text{ss}}$  stream. That means that vector  $\mathbf{x}^{(k)} = (x_{j_{\text{ss}}}^{(k)}, j_{\text{ss}} = 1 \dots N_{\text{ss}})$  is fed to all the  $N_{\text{ss}}$  streams simultaneously to be transmitted over the  $k$ th subcarrier in order to estimate MIMO channel matrix on the  $k$ th subcarrier frequency. Let's denote  $\hat{\mathbf{x}} = (\mathbf{x}_{j_{\text{ss}}}, j_{\text{ss}} = 1 \dots N_{\text{ss}})$ . To probe all the dimensions of the MIMO channel, not one but several  $\mathbf{X} = (\hat{\mathbf{x}}_{j_{\text{tof}}}, j_{\text{tof}} = 1 \dots N_{\text{tof}})$  are transmitted in the preamble (in sequence) where,  $N_{\text{tof}} \geq N_{\text{ss}}$ . In other words,  $N_{\text{tof}} \times N_{\text{ss}} \times N_{\text{sc}}$  two-state training symbols  $x_{j_{\text{ss}}}^{(k)}$  will have to be sent to learn  $N_{\text{rx}} \times N_{\text{ss}} \times N_{\text{sc}}$  complex coefficients of the MIMO channel [20]. Subsequently, a matrix  $\mathbf{Y}^{(k)}$  is received for the  $k$ th HT-LTF symbol on  $N_{\text{rx}}$  received antennas.

## III. CHALLENGES OF RANGING WITH CSI

In general, ToF estimation based on CSI suffers from several deep-rooted issues some of which have not been discussed in the literature. These issues are pointed out next and dealt with in detail later on.

a) **Bandwidth Limitation**: Range estimation has been traditionally done through derivation of the channel impulse response (CIR) for each tx/rx pair and hunting CIR's first and strongest peak. This simple approach has been effective in ranging with UWB radio and been lately pursued in the WiFi-based indoor localization literature [13], [18], [23]. Without delving into derivation details, CIR is obtained by taking the IFFT of the samples of the channel-frequency response (CFR), i.e. CSI metric, while accounting for the fact that no CSI is collected on  $k = 0$  (i.e. zero subcarrier)<sup>2</sup> and is given by

$$h^{(m)} = \sum_{j_{\text{mp}}=1}^{N_{\text{mp}}} \Gamma_{j_{\text{mp}}} \left( \frac{\sin\left(\frac{\pi(N_{\text{sc}}+1)}{N_{\text{sc}}}(\kappa_{j_{\text{mp}}} - m)\right)}{\sin\left(\frac{\pi}{N_{\text{sc}}}(\kappa_{j_{\text{mp}}} - m)\right)} - 1 \right) \quad (2)$$

where  $m$  is the time (delay) domain index and

$$\Gamma_{j_{\text{mp}}} = \frac{1}{N_{\text{sc}}} \beta_{j_{\text{mp}}} e^{-2\pi i f_0 \tau_{j_{\text{mp}}}} e^{\frac{\pi i (N_{\text{sc}}-1)}{N_{\text{sc}}} m} \quad \text{and} \quad \kappa_{j_{\text{mp}}} = N_{\text{sc}} \Delta f \tau_{j_{\text{mp}}}$$

where  $N_{\text{mp}}$ ,  $\tau_{j_{\text{mp}}}$ ,  $\beta_{j_{\text{mp}}}$ ,  $\Delta f$ ,  $f_0$  are the number of multipath arrivals, delay and attenuation on  $j_{\text{mp}}$ th path, subcarrier-spacing, and central frequency, respectively. This power-delay-profile (PDP) peaks at discrete samples  $m = m_{\text{peak}} = \lfloor \kappa_{j_{\text{mp}}} \rfloor$  only if (i)  $j_{\text{mp}}$ th arrival has enough strength  $|\Gamma_{j_{\text{mp}}}|$  (ii) close-by arrivals are not within each other's Rayleigh resolution limit, i.e.  $|\tau_{j_{\text{mp}}} - \tau_{j'_{\text{mp}}}| > 1/(N_{\text{sc}} \Delta f)$ . For WiFi systems with sampling rate 20Mega sample/s (MSPS) (for a  $B = 20\text{MHz}$  channel), the electromagnetic wave travels extra 15m between

<sup>1</sup>For example, for a 4x4 MIMO system, CDD values 0, -400, -200, -600ns are suggested. For WLAN systems operating on sampling rate  $T_s = 1/B = 50\text{ns}$ , where  $B = 20\text{MHz}$ , these CDDs are equivalent to delays equivalent to 0, 8, 4, 12 samples.

<sup>2</sup>Transmitting data on OFDM's center frequency would result in loss of information due to strong DC current at BB.

$$\begin{bmatrix} y_{1,1}^{(k)} & \cdots & y_{1,N_{\text{tff}}}^{(k)} \\ \vdots & \ddots & \vdots \\ y_{N_{\text{rx}},1}^{(k)} & \cdots & y_{N_{\text{rx}},N_{\text{tff}}}^{(k)} \end{bmatrix} = \begin{bmatrix} h_{1,1}^{(k)} & \cdots & h_{1,N_{\text{tx}}}^{(k)} \\ \vdots & \ddots & \vdots \\ h_{N_{\text{rx}},1}^{(k)} & \cdots & h_{N_{\text{rx}},N_{\text{tx}}}^{(k)} \end{bmatrix} \begin{bmatrix} \phi_{a,1,1}^{(k)} & \cdots & 0 \\ \vdots & \ddots & \vdots \\ 0 & \cdots & \phi_{a,N_{\text{tx}},N_{\text{tx}}}^{(k)} \end{bmatrix} \times \\
\begin{bmatrix} q_{1,1}^{(k)} & \cdots & q_{1,N_{\text{ss}}}^{(k)} \\ \vdots & \ddots & \vdots \\ q_{N_{\text{tx}},1}^{(k)} & \cdots & q_{N_{\text{tx}},N_{\text{ss}}}^{(k)} \end{bmatrix} \begin{bmatrix} \phi_{b,1,1}^{(k)} & \cdots & 0 \\ \vdots & \ddots & \vdots \\ 0 & \cdots & \phi_{b,N_{\text{ss}},N_{\text{ss}}}^{(k)} \end{bmatrix} \begin{bmatrix} x_k p_{1,1} & \cdots & x_k p_{1,N_{\text{tff}}} \\ \vdots & \ddots & \vdots \\ x_k p_{N_{\text{ss}},1} & \cdots & x_k p_{N_{\text{ss}},N_{\text{tff}}} \end{bmatrix} + \mathbf{N}_k \quad (3)$$

two consecutive samples. Such low sampling rate makes resolving closely-spaced multipath reflections (as needed for indoor positioning) based on CIR theoretically impossible.

**b) CSI Phase Contamination:** The phase in the CSI matrix is contaminated with terms triggered by the imperfect synchronization between the transmitter and receiver in analog/digital domains. Dubbed by the names symbol timing offset (STO), sampling frequency offset (SFO), carrier frequency offset (CFO), and carrier phase offset (CPO), these frequency and time synchronization errors are extremely volatile in nature [24].

**c) CSI Amplitude Contamination:** The amplitude of the CSI is highly distorted by three phenomena: (a) unpredictable changes in AGC gain, (b) I/Q imbalance, and (c) the mixed effect of cyclic-prefix removal/guard-band insertion/windowing operation on time-domain CSI samples.

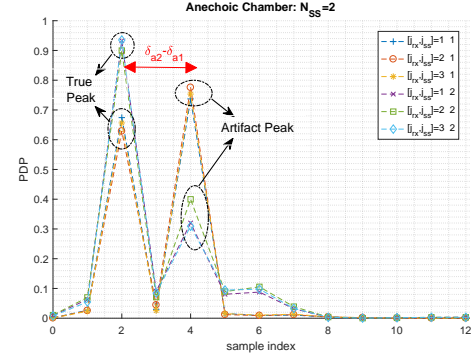
**d) CDD Phase Shift:** The CDD included in the CSI matrix appears as an additive phase in the CSI matrix. CDD can potentially degrade the ranging accuracy using CSI by several tens of meters. This is particularly the case when  $N_{\text{ss}} < N_{\text{tx}}$  [20], [21].

**e) Artificial Multipath:** The multiplexing operation  $\mathbf{Q}^{(k)}$  performed on input streams causes the received samples to look as if they were transmitted on a fading channel with many more reflections [20], [22].

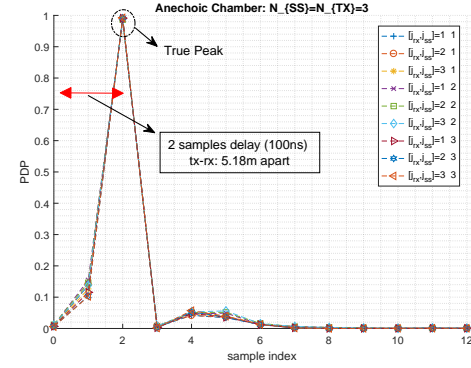
### A. Impact of OFDM Baseband Operations

**1) SMM and CDD:** Accounting for the SMM and CDD operations at the transmitter, the entire sounding mechanism can be described by (3), at the top of the page, where  $\mathbf{P}$  (the rightmost matrix) is called the orthogonal mapping matrix. The CSI matrix is calculated as  $\mathbf{CSI}^{(k)} = \mathbf{Y}^{(k)} \mathbf{P}^{-1}$ , for each subcarrier. In (3),  $\Phi_a$  and  $\Phi_b$  are the cyclic shift (diagonal) matrices before and after spatial mapping, which is denoted by  $\mathbf{Q}$ , a linear matrix, as shown in the transceiver architecture of Fig. 1 and  $\mathbf{N}_k$  is the noise matrix. Because  $\Phi_a$ ,  $\Phi_b$ ,  $\mathbf{Q}$  are implementation-dependent quantities, estimating matrix  $\mathbf{H}^{(k)}$  at the receiver from observations  $\mathbf{CSI}^{(k)}$  is challenging. However, the receiver does not require to extract the channel matrix  $\mathbf{H}^{(k)}$  to decode data points; so long as  $\Phi_a$ ,  $\Phi_b$ ,  $\mathbf{Q}$  are applied to both training sequences and payload (which is indeed the case), the receiver can view  $\hat{\mathbf{H}}^{(k)} = \mathbf{H}^{(k)} \Phi_a^{(k)} \mathbf{Q}^{(k)} \Phi_b^{(k)}$  as an end-to-end channel. Elaborating on (3), and given that the receiver removes the orthogonal mapping matrix  $\mathbf{P}$ , the  $(j_{\text{rx}}, j_{\text{ss}})$  element of the CSI matrix is given by

$$\text{csi}_{j_{\text{rx}},j_{\text{ss}}}^{(k)} = \sum_{j_{\text{tx}}=1}^{N_{\text{tx}}} h_{j_{\text{rx}},j_{\text{tx}}}^{(k)} \phi_{a,j_{\text{tx}},j_{\text{tx}}}^{(k)} q_{j_{\text{tx}},j_{\text{ss}}}^{(k)} \phi_{b,j_{\text{ss}},j_{\text{ss}}}^{(k)} + n_k \quad (4)$$



(a) Chamber,  $N_{\text{ss}} = 2$ .



(b) Chamber,  $N_{\text{ss}} = 3$ .

Fig. 2: Plots of PDP in anechoic chamber (Fig. 7c). For  $N_{\text{ss}} = 2 \rightarrow \mathbf{Q} \neq \mathbf{I}$  (left), hence, PDP exhibits extra artifact peak. No such peak is observed when  $N_{\text{ss}} = 3 \rightarrow \mathbf{Q} = \mathbf{I}$ . Yet, peaks in both scenarios are shifted by few samples due to the existence of STO, pre-advancement, or CDD.

where  $j_{\text{rx}}$ ,  $j_{\text{tx}}$ ,  $j_{\text{ss}}$  represent receive antenna, transmit antennas, and spatial stream indices, respectively. From (4), the information on the ToF of the line-of-sight (LoS) path is concealed in  $h_{j_{\text{rx}},j_{\text{tx}}}^{(k)}$  which is given by

$$h_{j_{\text{rx}},j_{\text{tx}}}^{(k)} = \sum_{j_{\text{mp}}=1}^{N_{\text{mp}}} \beta_{j_{\text{mp}}}^{j_{\text{rx}},j_{\text{tx}}} e^{-2\pi i f_k \tau_{j_{\text{mp}}}^{j_{\text{rx}},j_{\text{tx}}}} \quad (5)$$

where  $\beta_{j_{\text{mp}}}^{j_{\text{rx}},j_{\text{tx}}}$  and  $\tau_{j_{\text{mp}}}^{j_{\text{rx}},j_{\text{tx}}}$  are the attenuation and time delay of the  $j_{\text{mp}}$ th path between  $j_{\text{rx}}$ th receive and  $j_{\text{tx}}$ th transmit antennas, respectively. Also,  $N_{\text{mp}}$  is the number of multipath components and  $f_k = f_0 + k\Delta f$  is the  $k$ th subcarrier's frequency with  $\Delta f$  and  $f_0$  being the subcarrier spacing and the center frequency, respectively. To better understand the effect of CDD and SMM on range measurement, we per-

formed experiments in an anechoic chamber (Fig. 7c) wherein  $N_{\text{mp}} \approx 1$  (no multipath). In cases when the CSI matrix is not full rank, i.e.  $N_{\text{ss}} \neq N_{\text{tx}}$ , we expect  $\mathbf{Q}^{(k)} \neq \mathbf{I}$ . In this situation, the PDP yields more than one peak  $m_{\text{peak}} = \lfloor N_{\text{sc}} \Delta f \tau_0^{j_{\text{rx}}, j_{\text{tx}}} + \delta_{a j_{\text{tx}}} + \delta_{b j_{\text{rx}}} \rfloor$ ,  $j_{\text{tx}} = 1 \cdots N_{\text{tx}}$ , where  $\delta_{a j_{\text{tx}}}$ ,  $\delta_{b j_{\text{rx}}}$  are the cyclic shifts before and after spatial mapping on the  $j_{\text{tx}}$ th transmit chain and the  $j_{\text{rx}}$  spatial stream. This is indeed the case as shown in Fig. 2. Fig. 2a uses data collected from a setup where transmitter and receiver arrays directly face each other whereas, in Fig. 2b, the receiver is rotated by 90 degrees. The latter experiment was performed to understand whether we can achieve a full channel matrix ( $N_{\text{ss}} = 3$ ) in non-scattering anechoic chamber.

In Fig. 2a, PDP is plotted for those packets that encounter a channel with  $N_{\text{ss}} = 2$ . As expected, peaks of equal strength is observed (for all transmit-receive sub-channels) which cannot be justified by the echo-free nature of the propagation environment. This is not observed in Fig. 2b where  $N_{\text{ss}} = 3$  and the SMM is often non-existent (explained later on). Nevertheless, in both figures, peaks are shifted to the right by 2 samples which could be caused by STO, pre-advancement, or CDD.<sup>3</sup>

The conclusion here is that raw CSI is unusable. One has to derive channel-related terms from CSI metrics in order to do positioning, a fact that is often underappreciated in the field of CSI-based positioning.

2) *Time Domain Windowing*: In examining the CSI obtained in a controlled *conducted* test (Fig. 7d), and in the anechoic chamber, non-linearities of regular shape were observed in both phase and amplitude of CSI as shown in Fig. 4a and Fig. 4b. The symmetric phase and amplitude non-linearity  $W^{(k)} = \mathcal{F}\{w^{(m)}\}$  on CSI (after FFT operation at the receiver) advocates a real-time operation  $w^{(m)}$  (after IFFT operation at the transmitter). Importantly, this phase distortion can degrade the ranging accuracy. We claim that this effect arises due to the combination of time-domain windowing, cyclic-prefix (CP) removal, and guard-band insertion at the transmitter as shown in Fig. 3 and the logic is as follows: Wireless communications systems follow a block-wise design methodology where hierarchies of subsystems<sup>4</sup> are used at the transmitter and receiver. This approach works because of the linearity of the operation performed in each block, hence, an inner block (say channel-equalization) remains transparent to the outer block (say encoding-decoding). This reversibility is true for most operations along a wireless chain except a few, where CP insertion-removal is the most important one. When CP of the training sequence (from which CSI is calculated) is removed at the receiver, what passes through is a sequence that is windowed (in time domain) from tail but intact from head. That is because the rising head of the time-domain windows are often not long enough to get passed CP and split into the OFDM symbol, but the falling tail of that time-domain window will impact the tail of OFDM symbol. This effect causes the observed distortion.

<sup>3</sup>Note that transmitter-receiver are 5.18m apart in anechoic chamber experiment which should produce a peak at sample index "0".

<sup>4</sup>e.g. scrambling  $\rightarrow$  FEC encoding  $\rightarrow$  stream parsing  $\rightarrow$  interleaving  $\rightarrow$  mapper  $\rightarrow$  channel  $\rightarrow$  equalization  $\rightarrow$  de-mapper  $\rightarrow$  de-interleaving  $\rightarrow$  de-parser  $\rightarrow$  FEC decoder  $\rightarrow$  de-scrambler

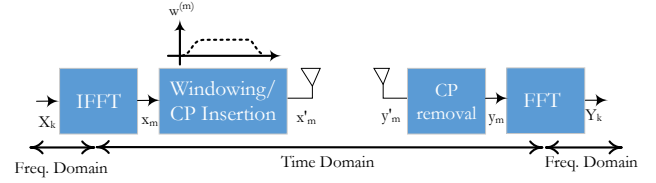


Fig. 3: Illustration of the mixed effect of windowing, CP removal, and guard-band insertion in SISO-OFDM system.

To further investigate this hypothesis, we worked on measurements collected in the *conducted* test setup. In this setting, and based on the model in (4),  $N_{\text{mp}} = 1$  and  $N_{\text{ss}} = N_{\text{tx}} \rightarrow \mathbf{Q} = \mathbf{I}$ , hence CSI with linear phase (vs  $k$ ) was expected, like  $\text{csi}_{j_{\text{rx}}, j_{\text{ss}}}^{(k)} = \gamma \exp(-2\pi i k \zeta / N_{\text{sc}}) + n_k$  where  $\zeta = N_{\text{sc}} \Delta f \tau_0^{j_{\text{rx}}, j_{\text{tx}}} + \delta_{a j_{\text{tx}}} + \delta_{b j_{\text{ss}}}$ , the latter two terms are the cyclic shifts after and before spatial mapping,  $\Delta f$  is the OFDM subcarrier spacing, and  $\gamma = \beta_0 \exp(-2\pi i f_0 \tau_0^{j_{\text{rx}}, j_{\text{ss}}})$  is a complex coefficient. Since the non-linearity is completely constant regardless of the choice of attenuators, cable length, etc., it implies a systematic operation happening in hardware. In fact, taking FFT of CSI yields  $\mathcal{F}_k^{-1}\{\text{csi}_{j_{\text{rx}}, j_{\text{ss}}}^{(k)}\} = \gamma \exp(\zeta_f) w^{(m-\zeta_I)}$  where  $\zeta_f$  and  $\zeta_I$  are the fractional and integer part of  $\zeta$ . This time-domain signal is plotted in Fig. 4c. This is a Tukey window as recommended in IEEE 802.11 standard [22].<sup>5</sup> Whereas the results for Atheros 93xx chipset are presented here, the same observation were made for Intel 53xx chipset. In the general case, the CSI model in (4) is revised as

$$\text{csi}_{j_{\text{rx}}}^{(k)} = \left( \sum_{j_{\text{tx}}=1}^{N_{\text{tx}}} \mathfrak{h}_{j_{\text{rx}}, j_{\text{tx}}}^{(k)} \phi_{a, j_{\text{tx}}, j_{\text{tx}}}^{(k)} \sum_{j_{\text{ss}}=1}^{N_{\text{ss}}} q_{j_{\text{tx}}, j_{\text{ss}}}^{(k)} \phi_{b, j_{\text{ss}}, j_{\text{ss}}}^{(k)} \right) |\tilde{W}^{(k)}| e^{i\angle \tilde{W}^{(k)}} + n_k \quad (6)$$

where

$$\tilde{W}^{(k)} = \mathcal{F} \left\{ w^{(m)} \cdot \text{rect}_{N_t}(m/N_{\text{sc}}) \right\} \otimes \text{rect}_{N_{\text{sc}}}(k/N_{\text{nz}})$$

and  $\text{rect}_{N_t}(m/N_{\text{sc}})$  is a time-domain rectangle function of length  $N_t = N_{\text{sc}} + N_{\text{cp}}$  to represent the CP removal operation on OFDM symbol,  $\text{rect}_{N_{\text{sc}}}(k/N_{\text{nz}})$  is a frequency-domain rectangle of length  $N_{\text{sc}} = N_{\text{nz}} + N_g$  to represent guard band insertion operation in OFDM systems, and  $w^{(m)}$  is the time-domain windowing function.  $N_{\text{cp}}$ ,  $N_g$ , and  $N_{\text{sc}}$  are the length of OFDM cyclic prefix (CP), the number of guard subcarriers, and the total number of subcarriers in OFDM system, respectively. Also  $\mathcal{F}(\cdot)$  and  $\otimes$  are the FFT and circular convolution operators. Since this is a deterministic effect that stems from a systematic design choice, a one-time non-linear fitting to the phase curve in Fig. 4a and de-rotating CSI phase accordingly would be sufficient without any concern with respect to over-fitting.<sup>6</sup>

*Discussion*: The existence of phase non-linearity in Fig. 4

<sup>5</sup>One should note that the Tukey window is a flat function with smooth edge falloff. However, the window we observe through CSI has an FFT whose  $N_g/2$  upper (and  $N_g/2$  lower) values are zeroed as a result of guard subcarrier exertion, which gives rise to Fig. 4c.

<sup>6</sup>Our fit is a 3rd-degree polynomial which resulted in  $-7 \cdot 10^{-5} k^3 + 3 \cdot 10^{-5} k^2 + 0.05 k$ .

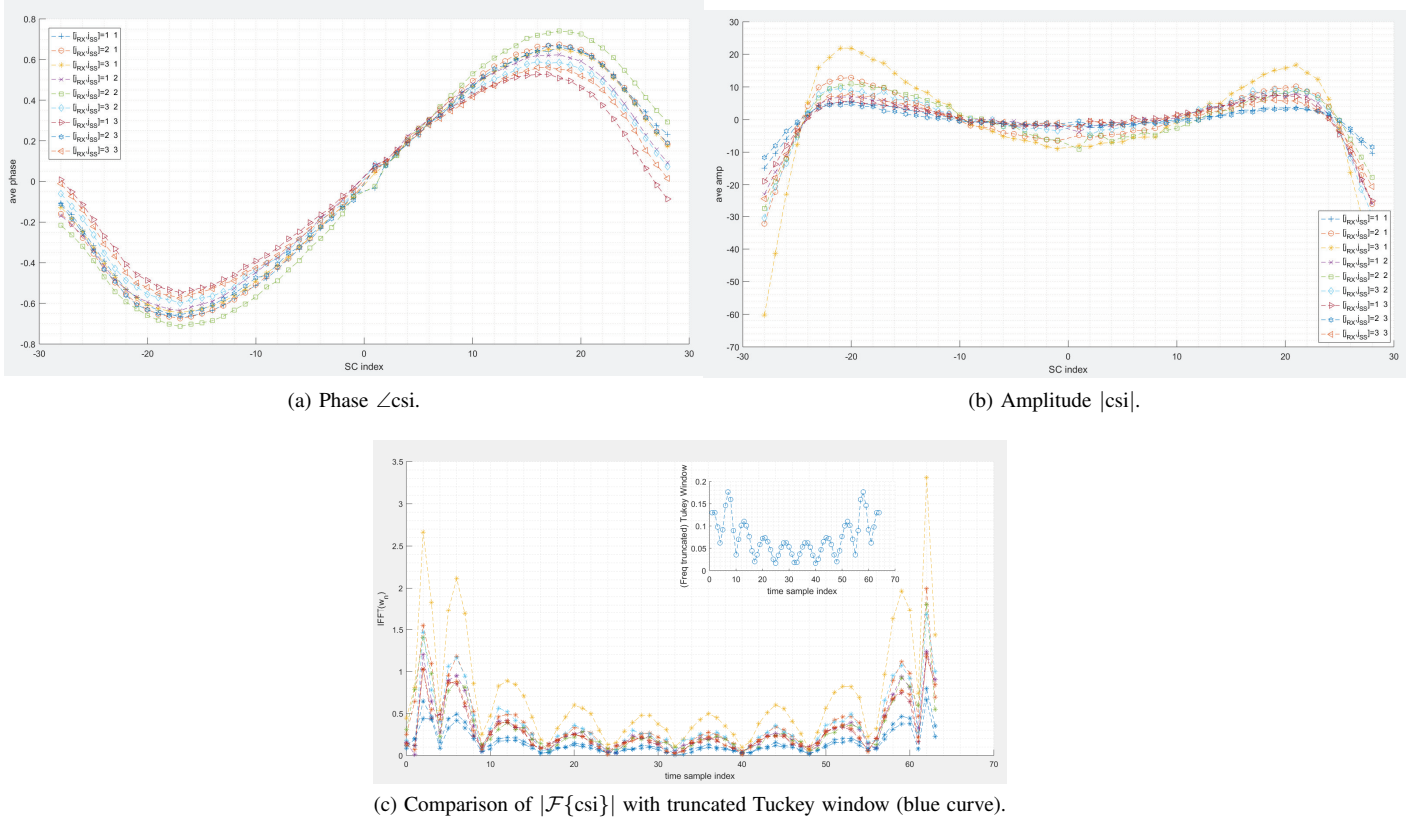


Fig. 4: Experimental results from conducted test measurements for (a)  $\angle \text{csi}$ , (b)  $|\text{csi}|$ , (c) and  $|\mathcal{F}\{\text{csi}\}|$  for different  $N_{ss}$  and  $N_{rx}$ . The similarity of the truncated Tuckey window (blue curve) to the experimental results in (c) corroborates that the non-linearities observed in (a) and (b) are due to the mixed effect of time-domain windowing, guard-band insertion, and CP removal.

has led some researchers to associate this with the I/Q imbalance phenomenon [25]. In several different works, e.g. [13], [23], [26], the trigonometric-like shape of the CSI phase (as depicted in Fig. 4) has led to incorrect representation of CSI as  $|\text{csi}^{(k)}| \exp(i \sin(\angle \text{csi}^{(k)}))$ . The unrecognised, deleterious effects of these baseband operations have led to the belief that CSI is not usable for ToF estimation and made range-based indoor positioning a less fruitful area of investigation. Chronos [5] is able to measure ToF by only using the zero subcarriers (at different frequency bands), a workaround that dodges all the deteriorations explained earlier. However, this is not the case if one needs to use CSI on arbitrary set of subcarriers for ToF estimation. On the other hand, estimating AoA using CSI circumvents these problems, as differencing the phases of the CSI at receive antennas eliminates the effect of the aforementioned additive phases imposed at the baseband of the transmitter [2]–[4].

### B. Impact of Imperfect Signal Processing

The matrix equation in (3) assumes perfect synchronization between the transmitter and receiver. Such assumption is not realistic as communication always suffers from lack of perfect time/frequency synchronization. To account for this, the CSI

model in (3) is revised as

$$\mathbf{CSI}^{(k)}(n) \leftarrow \mathbf{CSI}^{(k)} \underbrace{\begin{bmatrix} f(\psi_1(n), \psi_2(n)) & \cdots & 0 \\ \vdots & \ddots & \vdots \\ 0 & \cdots & f(\psi_1(n), \psi_2(n)) \end{bmatrix}}_{\Psi^{(k)}(n)} \quad (7)$$

where  $\mathbf{CSI}^{(k)}$  is given by (3),  $\Psi^{(k)}(n)$  is an  $N_{rx}$  by  $N_{rx}$  matrix of complex and time-dependent elements  $f(\psi_1(n), \psi_2(n)) = \exp(-i(k\psi_1(n) + \psi_2(n)))$  to account for phenomena such as symbol timing offset (STO), carrier frequency offset (CFO), sampling frequency offset (SFO), and carrier phase offset (CPO). Since the chains (transmit and receive) in today's MIMO systems are driven by one oscillator in an  $N_{rx} \times N_{tx}$  MIMO system, every pair of transmit-receive ports ( $n_{rx}, n_{tx}$ ) observe similar synchronization error in (7). Please note the difference between the time index  $n$  in (7) (to distinguish CSI for different packets) and delay index  $m$  in (2) (to distinguish discrete multipath components of the channel).

In general,  $\Psi^{(k)}(n)$  can be an arbitrary matrix with non-zero elements. However, when there is no coupling between receiver chains, this matrix will be diagonal. Also given that all RF chains in MIMO WLAN systems use a common oscillator/synthesizer, the complex diagonal elements of  $\Psi^{(k)}(n)$  are the same. Our extensive experiments in the anechoic chamber (Fig. 7c) verifies the following two hypotheses regarding the phase of  $f(\cdot, \cdot)$ : (i) linear in subcarrier index (ii) highly

variable even in purely static environment. These additive phase terms highly degrade the accuracy of the CSI-based ranging as reported in several localization studies [2], [3], [5] and are discussed next.

1) *Frequency Errors*: In down-converting analog passband (PB) signal to baseband (BB), the following errors are introduced into the CSI:

- **CFO/CPO**: The generated carrier at the receiver can be represented by a complex exponential. CFO exists when the receiver's carrier frequency  $f'_0$  drifts from the transmitted carrier frequency  $f_0$  by  $\Delta_c = f'_0 - f_0$  due to residual errors in receiver's phase locked loop (PLL).<sup>7</sup> On the other hand, CPO  $\phi_c$  is imposed because receiver's voltage controlled oscillator (VCO) starts from a random phase every time the synthesizer restarts and the phase locked loop (PLL) cannot completely compensate for the phase difference between generated carrier and received signal. Both of these effects are shown to affect CSI in the following manner

$$\hat{\text{csi}}_{j_{\text{rx}}, j_{\text{ss}}}^{(k)}(n) = \text{csi}_{j_{\text{rx}}, j_{\text{ss}}}^{(k)}(n) e^{-2\pi i \left( \frac{\zeta_{\text{CFO}} \cdot g_2(n)}{N_{\text{sc}}} + \phi_c \right)} + n_k \quad (8)$$

where  $\zeta_{\text{CFO}} = (f'_0 - f_0)/\Delta f$  is the CFO normalized with OFDM subcarrier spacing  $\Delta f$ . Equation (8) signifies an additive phase that is cumulative in time as denoted by  $g_2(n)$ . Due to its accumulative nature, CFO is regularly tracked by the receiver and compensated for. However, the residual leftover can be detrimental in precise ranging.

2) *Timing Errors*: These errors happen when receiver (transmitter) samples (synthesizes) signals at mismatching rates. There is also the significant issue of symbol boundary detection as discussed next:

- **SFO**: In modern homodyne architectures, the same oscillator triggering the mixer drives the analog-to-digital converter (ADC). If the ADC samples the received signal with rate  $T'_s$  different from transmitter's synthesization rate  $T_s$ , SFO is experienced. This is manifested as an additive phase shift proportional to the subcarrier index and cumulative in time [24], [27]. Mathematically,

$$\hat{\text{csi}}_{j_{\text{rx}}, j_{\text{ss}}}^{(k)}(n) = \text{csi}_{j_{\text{rx}}, j_{\text{ss}}}^{(k)}(n) e^{-2\pi i k \left( \frac{\zeta_{\text{SFO}} \cdot g_1(n)}{N_{\text{sc}}} \right)} + n_k \quad (9)$$

where  $\zeta_{\text{SFO}} = (T'_s - T_s)/T_s$  is the SFO normalized with the sampling time and  $g_1(n)$  denotes the SFO calibration interval.

- **STO**: STO is the most degrading effect arising due to the lack of knowledge about the beginning of the received OFDM symbol [24]. This uncertainty emerges as it is not a-priori known when to expect a packet. Since OFDM systems function on blocks of (time domain) samples, named symbols, it is crucial that the right block is fed to the FFT demodulator. To find out about the symbol boundary, header starts with known, periodic

<sup>7</sup>The CFO can also be due to Doppler effect. Nonetheless, contribution of the latter to  $\Delta_c$  is considerably less compared to oscillator frequency mismatch.

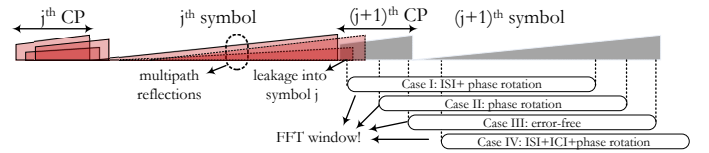


Fig. 5: Two consecutive OFDM symbols  $j$  and  $j+1$  are shown with a triangle. Overlapping triangles reflect multipath effect. Different choices of OFDM FFT window (a.k.a. symbol boundary) lead to four types of deteriorations in detecting symbol  $j+1$ .

sequences (named short-training fields-STF) and auto-correlator/cross-correlator is utilized at the receiver to capture and detect the presence of WiFi signals. However, because of the length limitations of these sequences, error in determining symbol boundary cannot be fully eliminated leading to irreversible errors such as inter-carrier interference (ICI), inter-symbol interference (ISI), and phase rotation, as seen in Fig. 5.<sup>8</sup> This phase rotation can be shown to impact CSI in the following manner:

$$\hat{\text{csi}}_{j_{\text{rx}}, j_{\text{ss}}}^{(k)}(n) = \text{csi}_{j_{\text{rx}}, j_{\text{ss}}}^{(k)}(n) e^{-2\pi i \left( \frac{k N_{\text{STO}}(n)}{N_{\text{sc}}} \right)} + n_k \quad (10)$$

- **OFDM Pre-advancement**: Accounting for STO uncertainty, and to avoid irrevocable ICI/ISI, almost all NIC chipsets intentionally (upon estimating symbol boundary) borrow  $\epsilon^{\text{pre}}$  samples from current OFDM symbol's CP. This operation, named pre-advancement, guarantees that FFR input samples are ISI/ICI free, and only (clockwise) cyclically shifted (Case II in Fig. 5) which creates phase rotation after FFT given by:<sup>9</sup>

$$\hat{\text{csi}}_{j_{\text{rx}}, j_{\text{ss}}}^{(k)} = \text{csi}_{j_{\text{rx}}, j_{\text{ss}}}^{(k)} e^{-2\pi i \left( \frac{k \epsilon^{\text{pre}}}{N_{\text{sc}}} \right)} + n_k \quad (11)$$

*Discussion*: Positioning based on the unprocessed CSI will be severely impacted as  $N_{\text{STO}} + \epsilon^{\text{pre}} = 1$  will cause 15m ranging inaccuracy at best. This is evident from our experimental measurements in Fig. 2: Whereas in the chamber the transmitter and receiver were 5m apart, calling for a PDPs that climax at the very first sample ( $n = 0$ ), the true peak actually happens at the third sample, an anomalous behaviour that is a testimony to the deliberate clockwise (left) cyclic shifting of OFDM symbol.

Accounting for non-idealities due to AGC, CFO, CPO, SFO, STO, and pre-advancement, the CSI model is revised

<sup>8</sup>ISI is experienced in case I of Fig. 5 because there is multipath leakage from  $j$ th symbol into the FFT window of the  $j+1$ th symbol. This is different from Case IV where not only leakage from the next symbol (i.e.  $j+2$  which is not plotted) causes ISI, but there is ICI as well since the FFT window is missing the beginning of OFDM frame. To summarize, FFT window should neither advance too much into CP (to avoid ISI with the previous symbol) nor should it progress into main part of OFDM symbol (to avoid ICI and ISI with the next symbol).

<sup>9</sup>pre-advancement won't impact decoding quality as both payload and channel estimation (HT-LTF) symbols undergo the same shift, hence equalization removes it.

as follows

$$\hat{\text{csi}}_{j_{\text{rx}},j_{\text{ss}}}^{(k)}(n) = \alpha_{\text{agc}} \text{csi}_{j_{\text{rx}},j_{\text{ss}}}^{(k)} \underbrace{\left( e^{-2\pi i \phi_c} \right)}_{\text{CPO}} \underbrace{\left( e^{-\frac{2\pi i \zeta_{\text{CFO}} g_2(n)}{N_{\text{sc}}}} \right)}_{\text{CFO}} \times \underbrace{\left( e^{-\frac{2\pi i k \zeta_{\text{SFO}} g_1(n)}{N_{\text{sc}}}} \right)}_{\text{SFO}} \underbrace{\left( e^{-\frac{2\pi i k (N_{\text{STO}} + \epsilon^{\text{Pfc}})}{N_{\text{sc}}}} \right)}_{\text{STO+pre-advancement}} + \mathcal{J}_k \quad (12)$$

where, according to Eq. (4),  $\text{csi}_{j_{\text{rx}},j_{\text{ss}}}^{(k)}$  is given by

$$\text{csi}_{j_{\text{rx}},j_{\text{ss}}}^{(k)} = \sum_{j_{\text{tx}}=1}^{N_{\text{tx}}} h_{j_{\text{rx}},j_{\text{tx}}}^{(k)} \phi_{a_{j_{\text{tx}},j_{\text{tx}}}}^{(k)} q_{j_{\text{tx}},j_{\text{ss}}}^{(k)} \phi_{b_{j_{\text{ss}},j_{\text{ss}}}}^{(k)} + n_k$$

The additive term  $\mathcal{J}_k$  entails noise  $n_k$ , ISI, and ICI. Despite its sophisticated look, the multiplicative error terms in (12) can be compactly represented by  $\exp(-i(k\psi_1(n) + \psi_2(n)))$  as initially claimed in (7).

#### IV. CSI CALIBRATION

We have discussed so far that ranging based solely on CSI is a futile effort unless (i) the effect of deterministic SMM, CDD, and mixed windowing operations are cancelled out (ii) random phase errors due to the lack of synchronization are compensated for.

In the following, we investigate the statistical behaviour of the CSI random phase errors and introduce techniques to remove them. Our goal is to estimate synchronization errors in (12) in the aforementioned onerous problem where errors are changing from packet to packets, thus, rendering classic estimation (ML, MMSE, etc.) approaches that rely on availability of many samples unusable.

##### A. Statistical Error Characterization

Due to the highly volatile nature of phase errors, differencing across time keeps the volatility while eliminating stagnant channel terms.<sup>10</sup> Doing so for consecutive CSI samples and performing phase unwrapping (w.r.t the subcarrier index  $k$ ) yields<sup>11</sup>

$$\begin{aligned} & \underbrace{\text{uwrp}_k \left[ \angle \text{csi}_{j_{\text{rx}},j_{\text{ss}}}^{(k)}(n_1) - \angle \text{csi}_{j_{\text{rx}},j_{\text{ss}}}^{(k)}(n_2) \right]}_{\Delta(\angle \text{csi}^{(k)})_{(n_1,n_2)}} \\ &= \text{uwrp}_k \left[ \underbrace{(\psi_1(n_1) - \psi_1(n_2))k}_{\Delta\psi_1(n_1,n_2)} + \underbrace{(\psi_2(n_1) - \psi_2(n_2))}_{\Delta\psi_2(n_1,n_2)} \pmod{2\pi} \right] \\ &= \text{uwrp}_k \left[ \Delta\psi_1(n_1,n_2)k \pmod{2\pi} \right] + \Delta\psi_2(n_1,n_2) \pmod{2\pi} \end{aligned} \quad (13)$$

where  $\text{uwrp}_k[\cdot]$  is phase unwrapping w.r.t to  $k$  and  $n_1$  and  $n_2$  are arbitrary time indices with the constraint that  $(|n_2 - n_1|T_s < T_c)$  with  $T_c$  being the coherence time of the channel. Also,  $x \pmod{2\pi}$  is the modulo operation, which is denoted by  $[x]_{2\pi}$ , hereinafter. To gain insights into the statistical nature of  $\psi_{1(2)}(n)$ , we use the measurements collected in an anechoic chamber. Fig. 6b shows CSI phase difference vs. subcarrier

<sup>10</sup>As a rough figure, the parameters of the indoor wireless channel change in the order of tens of ms.

<sup>11</sup>One has to be wary of the fact that we do not get to observe  $\Delta\psi_1 k + \Delta\psi_2$  but its  $2\pi$  modulus.

index for two cases: (i)  $N_p = 12$  (ii)  $N_p = 8000$  CSI measurements. Fig. 6c displays the empirical PDF of  $\Delta\psi_r$ ,  $r = \{1, 2\}$ , for  $N_p = 8000$ . The following conclusions are drawn:

- Even for as low as  $N_p = 12$ , the randomness introduced by  $\psi_r(n)$ ,  $r = \{1, 2\}$  is so large that it drives the average phase difference (horizontal red line) to zero. This observation substantiates that both  $[\Delta\psi_1(n_1, n_2)]_{2\pi}$  and  $[\Delta\psi_2(n_1, n_2)]_{2\pi}$  are zero mean random processes.
- The obvious linearity in Fig. 6b conforms with the derivations in (12) as was reported in earlier works [18].
- The drastic changes of  $\Delta(\angle \text{csi}^{(k)}) = [k\Delta\psi_1 + \Delta\psi_2]_{2\pi}$  is because of two effects: (a) The high dynamicity of receiver's synchronization algorithms (b) the  $\angle(\cdot)$  operation which delivers not the true angle but the wrapped-around version of it.
- The Gaussianity of  $\Delta\psi_r$ ,  $r = \{1, 2\}$  is proved as follows: Since  $\Delta(\angle \text{csi}^{(k)})$  is a Gaussian process (per our observation),  $\Delta(\angle \text{csi}^{(k=0)}) = \Delta\psi_2$  is Gaussian random variable. Noting that  $\Delta\psi_1 \perp \Delta\psi_2$ , then  $\varphi_{k_0 \Delta\psi_1}(t) \cdot \varphi_{\Delta\psi_2}(t) = \varphi_{\Delta(\angle \text{csi}^{(k_0)})}(t)$ , where  $\varphi_a(t)$  is the characteristic function of random variable  $a$ . Subsequently, the PDF of  $\Delta\psi_1$  is attained using the Fourier transform, that is,  $f_{\Delta\psi_1} = 1/k_0 \mathcal{F}\{\varphi_{\Delta(\angle \text{csi}^{(k_0)})}(t)/\varphi_{\Delta\psi_2}(t)\}$  which can be shown to be a Gaussian. This is shown in Fig. 6c.
- Finally, the knowledge of  $\Delta\psi_r = \mathcal{N}(0, \sigma_r^2)$  implies  $\psi_r = \mathcal{N}(\mu_{1(2)}, \sigma_r^2/2)$ ,  $r = \{1, 2\}$ . This is true since the process  $\psi_r(n)$  has the same distribution for different  $n$ . Yet, so long as the cyclic-prefix (CP) pre-advancement is performed at the receiver, deeming  $\psi_r(n)$  as a zero-mean random variable [18] yields completely biased range estimates.

*Discussion:* These findings contradict some views on the uniformity of distributions  $\psi_r$  [28], [29], an assertion seemingly made due to equating the statistical behaviour of  $[\psi_r]_{2\pi}$  with that of  $\psi_r$ .

##### B. Estimating STO and SFO

The unpredictability of phase errors  $\psi_1(n)$  in (12) stems from the following reasons:

- Randomness in  $g_1(n)$  due to the opportunistic nature of WLAN access protocol.
- Randomness in  $g_1(n)$  due to receiver's ability to initiate calibration using any packet header on the air regardless of whether it was destined to it or not.
- Errors in estimating the amount of drift  $\zeta_{\text{SFO}}$  which depends on how badly the calibrating header is influenced by small scale fading.
- Errors in estimating the symbol boundary and  $N_{\text{STO}}$  which, again, depends on the fading nature of the channel.
- OFDM pre-advancement [20].

For these reasons,  $\psi_1(n)$  is decorrelated for different  $n$ . Therefore, only CSI across frequency and space can be used to estimate  $\psi_1(n)$ . With this knowledge and given the linearity of the additive phase (in  $k$ ) in (12), several previous works [2], [30], [31] adopted a simple CSI phase de-trending to eliminate



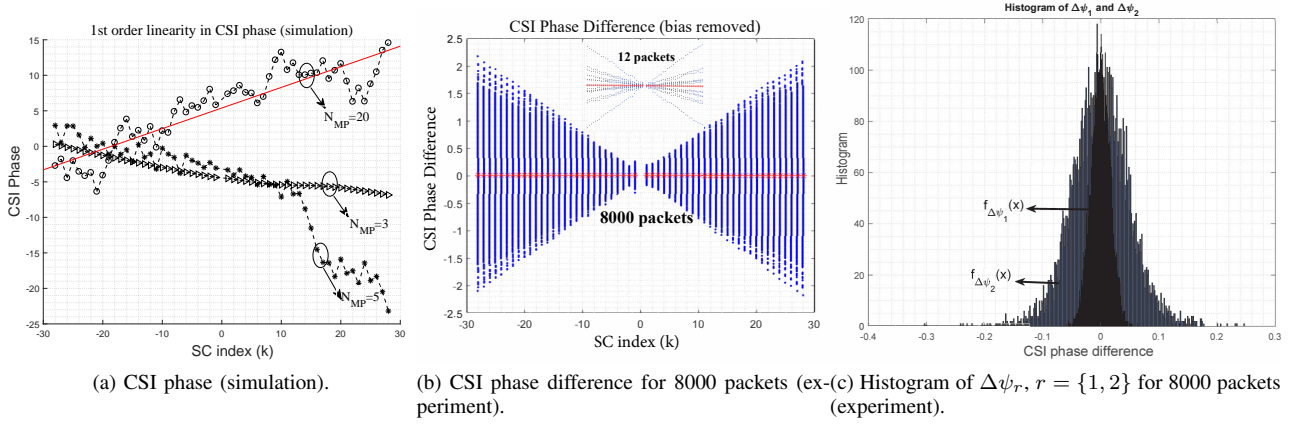


Fig. 6: (a) simulation: This figure proves that channel phase has affine component (red straight line)  $N_{mp} = 3, 5, 20$ . (b) experiment: differencing phase of CSI of consecutive packets in (12) eliminates channel component while keeping the volatile synchronization component. This figure also proves that linearity (vs.  $k$ ) is a valid assumption for  $\Delta(\angle \text{csi}^{(k)})$ . Moreover,  $\Delta(\angle \text{csi}^{(k)})$  is a zero mean random variable whose mean is shown by the red horizontal line. (c) experiment: histogram of  $\Delta\psi_r$ ,  $r = \{1, 2\}$  corroborates the validity of Gaussian assumption.

$\psi_1(n)$ . This estimator can more generally be expressed as

$$\hat{\psi}_1(n) = -\angle \frac{1}{(N_{nz} - 1)} \sum_{k=-N_{nz}/2+1}^{N_{nz}/2} \left( \text{csi}_{j_{rx}, j_{ss}}^{(k)}(n) \text{csi}_{j_{rx}, j_{ss}}^{(k-1)*}(n) \right) \quad (14)$$

where  $\text{csi}_{j_{rx}, j_{ss}}^{(k)}$  is the  $(j_{rx}, j_{ss})$ th element of the CSI matrix,  $N_{nz} = N_{sc} - N_g$  is the number of non-zero subcarriers and  $N_g$  is the number of guard subcarriers at both ends of spectrum that are not used to modulate any symbol. This is an exact estimator, i.e.  $\psi_1(n) = \hat{\psi}_1(n)$ , only when (i) the channel does not change variably between two adjacent subcarriers, that is  $\text{h}_{j_{rx}, j_{tx}}^{(k)} \text{h}_{j_{rx}, j_{tx}}^{(k-1)*} \approx |\text{h}_{j_{rx}, j_{ss}}^{(k)}|^2$  and (ii)  $\mathbb{E}\{\psi_1(n)\} = 0$ .

None of these two conditions is satisfied in reality: As shown in Fig. 6a, the true channel phase normally has a first-order linearity, hence, (14) estimates  $\psi_1$  plus the linear phase term in  $\text{h}_{j_{rx}, j_{tx}}$ , which is denoted by  $\epsilon_{j_{rx}, j_{tx}}^{\text{ch}}$  hereinafter. In this situation, (14) becomes (often negatively) a biased estimator and compensating CSI using it (as in (16)) gravely impacts ranging accuracy possibly worse than keeping STO and ranging with the original CSI. The performance of (14) is studied for thousands of channel realizations and for two different STO+SFO drift. The bias of the estimator, caused by eliminating the first-order channel linearity  $k \cdot \epsilon_{j_{rx}, j_{tx}}^{\text{ch}}$  was observed.

1) *Alternative Estimators*: In obtaining  $\hat{\psi}_1(n)$ , the following estimator was proven more effective in reducing the estimation error in lieu of (14).

a) *Spatial/spectral Averaging*: Given that all transmit/receive sub-channels experience the same hardware error, averaging can be performed in those dimensions as follows:

$$\hat{\psi}_1^{(1)}(n) = -\angle \left( \frac{1}{(N_{nz} - 1) N_{rx} N_{ss}} \sum_{k=-N_{nz}/2+1}^{N_{nz}/2} \sum_{j_{rx}=1}^{N_{rx}} \sum_{j_{ss}=1}^{N_{ss}} \text{csi}_{j_{rx}, j_{ss}}^{(k)}(n) \text{csi}_{j_{rx}, j_{ss}}^{(k-1)*}(n) \right) \quad (15)$$

Having obtained  $\hat{\psi}_1$ , compensation is performed with simple

post multiplication with the CSI matrix as follows,

$$\tilde{\text{CSI}}^{(k)}(n) = e^{i(\hat{\psi}_1(n))k} \cdot \text{CSI}^{(k)}(n) \quad (16)$$

### Algorithm 1 1st-Order Linearity Removal

---

**Input:**  $\text{CSI}^{(1:N_{sc})}(1 : N_p)$   
**Output:**  $\text{CSI}^{(1:N_{sc})}(1 : N_p)$   
**procedure** COMPENSATION1(**Input**)  
 De-rotate  $\angle \text{CSI}^{(1:N_{sc})}(1 : N_p)$  by  $-7e - 5k^3 + 3e - 5k^2 + 0.05k$   $\triangleright$   
 Windowing/CP removal effect compensation  
 $s = 0$ ,  $\text{flag} = 0$ ;  
 $\mathcal{A}$  :  $\triangleright$  Return here to compensate for channel-linearity  
**for**  $j_p = 1 : N_p$  **do**  
**if**  $\text{flag} == 0$  **then**  
 Estimate  $\hat{\psi}_1(j_p)$  using (14) or (15);  
 $s = s + \hat{\psi}_1(j_p)$ ;  
**else**  
 $\tilde{\psi}_1(j_p) \approx \hat{\psi}_1(j_p) - \epsilon_{j_{rx}, j_{tx}}^{\text{ch}}$ ;  
 $\text{CSI}^{(1:N_{sc})}(j_p) = \text{Derotate}(\text{CSI}^{(1:N_{sc})}(j_p), \tilde{\psi}_1(j_p))$ ;  
 $\triangleright$  De-rotate CSI phase using (16)  
**end if**  
**end for**  
 $\epsilon_{j_{rx}, j_{tx}}^{\text{ch}} = s / N_p$ ;  
 $\text{flag} = 1$ ;  
**Goto**  $\mathcal{A}$   $\triangleright$  Return to  $\mathcal{A}$  only once  
**end procedure**

---

2) *Recovering Channel Phase Linearity*: The goal is to subtract the first-order channel linearity  $\epsilon_{j_{rx}, j_{tx}}^{\text{ch}}$  that is removed (along with phase errors) in (14)-(15). However, unless the true attenuations  $\beta$ , path delays  $\tau$ , and  $N_{mp}$  are precisely known in advance (which is actually the ultimate goal of positioning), no deterministic approach can find  $\epsilon_{j_{rx}, j_{tx}}^{\text{ch}}$ . Yet, with the knowledge that the channel-related term remains constant over the course of several packets, and leveraging the randomness in  $\psi_1$ , Algorithm 1 is used to remove the volatility contributed by SFO and find  $\hat{\psi}_1(n)$ . This is corroborated when observing that  $\hat{\psi}_1(n)$  is closely independent of  $j_{rx}$  and  $j_{tx}$  (which is expected as per (12)) whereas  $\psi_1(n)$  varies across antennas.



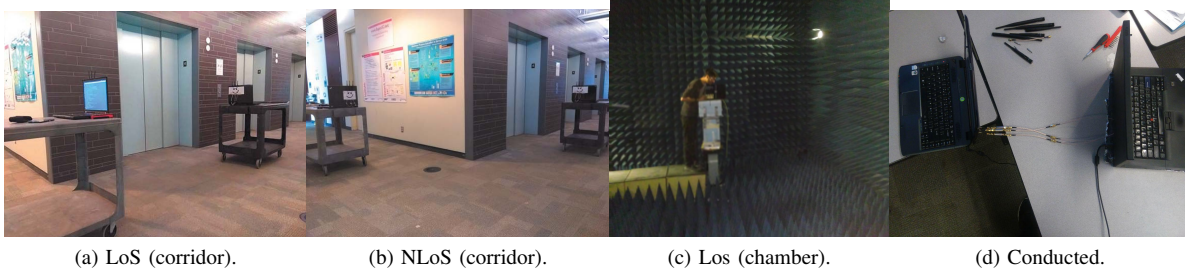


Fig. 7: Different test setup investigated in this research.

among the hypothesis set  $\mathcal{D} = \{\hat{d}, \hat{d} + 15m, \hat{d} + 30m, \dots\}$ . Since we also have access to the received power through RSSI metric and knowing that several dB of power loss is expected as distance increases by 15m,<sup>13</sup> almost all of these hypotheses in  $\mathcal{D}$  are rejected except one. This idea is better illustrated in Fig. 8. Briefly, all the hypotheses are formed and, then, examined based on the matching between the tabulated RSSI (collected in offline phase) and the observed RSSI (collected in online phase). In the example of Fig. 8, this approach chooses  $\hat{d} + 30 = 36m$  as the range estimate instead of the initial  $\hat{d} = 6m$ .<sup>14</sup>

### E. Removing Baseband Effects

Having eliminated the synchronization sources of error, the CSI output of Algorithm 3 is given by

$$\check{\text{csi}}_{j_{rx}, j_{ss}}^{(k)} = \sum_{j_{tx}=1}^{N_{tx}} e^{-\frac{2\pi i k (\delta_a j_{tx} + \delta_b j_{ss})}{N_{sc}}} h_{j_{rx}, j_{tx}}^{(k)} q_{j_{tx}, j_{ss}}^{(k)} + n_k \quad (17)$$

As discussed before, CDD affects ranging as if transmitter/receiver are farther away from each other.<sup>15</sup> On the other hand, SMM makes the receiver believe that there are more multipath arrivals than there really is. While it might appear that removing CDD/SMM is a trivial task, this is an implementation-dependent matter whereof details are not always available from the chipset manufacturers. As a matter of fact, the same chipset might use different CDDs at different times. Luckily, our experiments in a conducted test setup with both Intel and Atheros chipset shows that when the channel is full rank, direct mapping takes place, where  $\mathbf{Q}^{(k)} = \mathbf{I}$ , and CDD is always removed by the receiver. This has not been the case when  $N_{ss} < N_{tx}$ .

In conclusion, when  $N_{ss} = N_{tx}$ , the CSI matrix  $\mathbf{CSI}^{(k)}$  is the closest to the channel matrix  $\mathbf{H}^{(k)}$  whose elements are given by

$$\check{\text{csi}}_{j_{rx}, j_{tx}}^{(k)} = h_{j_{rx}, j_{tx}}^{(k)} = \sum_{j_{mp}=1}^{N_{mp}} \beta_{j_{mp}}^{j_{rx}, j_{tx}} \cdot e^{-2\pi i f_k \tau_{j_{mp}}^{j_{rx}, j_{tx}}} + n_k \quad (18)$$

<sup>13</sup>The exact power reduction due to path-loss depends on many factors. Per our observation, doubling the distance results in 5 – 10dB power reduction

<sup>14</sup>Note that RSSI is a relative index. Each chipset manufacturer can define their own ‘‘RSSI-Max’’ value. Cisco, for example, Cisco uses a 0 – 100 scale, while Atheros uses 0 – 60. Nonetheless, the higher the RSSI value is, the better the signal is. In case of Atheros,  $\text{RSSI} = 95 + E(\text{dbm})$ , where  $E$  is the received signal energy.

<sup>15</sup>For instance, with sampling time  $T_s = 50\text{ns}$  (in case of IEEE802.11n WLANs), a  $d = 400\text{ns}$  cyclic shift is equivalent to  $\delta = d/T_s = 8$

## V. CSI-BASED TOF ESTIMATION

### A. Spectral-Domain MUSIC Algorithm

Having cleaned the CSI samples from random and deterministic errors, our goal in this section is to use them to obtain range estimates. As discussed before, estimating the ToF of the signal using PDP has limited resolution due to bandwidth limitations of WiFi signals. On the other hand, [32] discovered that the subspace-based MUSIC algorithm that was traditionally used to estimate the AoA of the signal can also be used to estimate the ToF of the signal. The inherent appeal of MUSIC algorithm for ranging lies in the fact that its resolution is not only determined by the signal bandwidth but also the total signal-to-noise ratio (SNR). For that reason, MUSIC is among *super-resolution* algorithms. For more comprehensive treatment of the topic, readers are referred to [32]–[34]. MUSIC leverages the structure of the received samples in (18) to form

$$\check{\text{csi}} = \mathbf{A} \cdot \gamma + \mathbf{n} \quad (19)$$

where  $\check{\text{csi}} = [\check{\text{csi}}^{(1)} \dots \check{\text{csi}}^{(N_{nz})}]^T$  is a vector of frequency domain post-processed CSI samples and  $\hat{\text{csi}} = \mathbf{A} \cdot \gamma$  is the noise-free CSI vector. Based on (18), the steering matrix  $[\mathbf{A}]_{N_{nz} \times N_{mp}}$ , steering vector  $[\mathbf{a}(\tau_{j_{mp}})]_{N_{nz} \times 1}$ , source vector  $[\gamma]_{N_{mp} \times 1}$ , and noise vector  $[\mathbf{n}]_{N_{nz} \times 1}$  are given by

$$\begin{aligned} \mathbf{A} &= [\mathbf{a}(\tau_1) \dots \mathbf{a}(\tau_{N_{mp}})] \\ \text{where } \mathbf{a}(\tau_{j_{mp}}) &= [1, e^{-2\pi i \Delta f \tau_{j_{mp}}}, \dots, e^{-2\pi i (N_{nz}-1) \Delta f \tau_{j_{mp}}}]^T \\ \gamma &= [\gamma_1 \dots \gamma_{N_{mp}}]^T \\ \gamma_{j_{mp}} &= \beta_{j_{mp}} e^{-2\pi i f_0 \tau_{j_{mp}}} \quad \text{and} \quad \mathbf{n} = [n_1 \dots n_{N_{nz}}]^T \end{aligned} \quad (20)$$

Assuming independence of noise  $\mathbf{n}$  from the signal  $\gamma$  in (19) and  $N_{nz} > N_{mp}$ , the covariance matrix of  $\check{\text{csi}}$  is given by  $\mathbf{R}_{\check{\text{csi}}} = \mathbf{R}_{\hat{\text{csi}}} + \mathbf{R}_{\mathbf{n}}$  where the noise-free CSI covariance matrix  $\mathbf{R}_{\hat{\text{csi}}} = \mathbf{A} \mathbf{R}_{\gamma} \mathbf{A}^H$  is only of rank  $N_{mp}$  (rank deficient). Therefore, the largest  $N_{mp}$  eigenvalues in decomposition  $\mathbf{R}_{\check{\text{csi}}} = \mathbf{E} \mathbf{\Lambda} \mathbf{E}^H$  are due to signal (multipath arrivals) and the rest are due to noise. This observation is then used to separate the noise subspace from the signal subspace by forming the following pseudo-spectrum

$$\text{PS}(\tau) = \frac{\mathbf{a}(\tau)^H \mathbf{a}(\tau)}{\mathbf{a}(\tau)^H \mathbf{E}_n \mathbf{E}_n^H \mathbf{a}(\tau)} \quad (21)$$

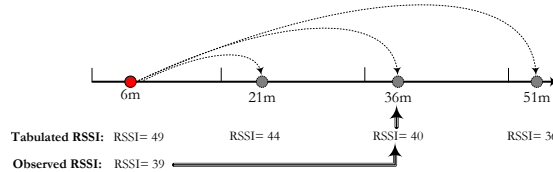


Fig. 8: Pictorial representation of RSSI assists accurate ranging estimation. Matching between the tabulated RSSI and the current packet's RSSI is used to find the true range estimate

which ideally peaks at about  $\tau = \tau_1 \cdots \tau_{N_{\text{mp}}}$  (if multipaths are sufficiently apart). In (21),  $\mathbf{E}_n = [\mathbf{e}_1, \cdots, \mathbf{e}_{N_{\text{nz}} - N_{\text{mp}}}]$  are the noise eigenvectors corresponding to  $N_{\text{nz}} - N_{\text{mp}}$  smallest eigenvalues of  $\mathbf{R}_{\text{csi}}$ . For the MUSIC algorithm to work, the following conditions are to be met [34]:

- (i)  $N_{\text{sc}} > N_{\text{mp}}$  and  $\mathbf{a}(\tau_{j_{\text{mp}}}) \nparallel \mathbf{a}(\tau'_{j_{\text{mp}}}), \forall j_{\text{mp}} \neq j'_{\text{mp}}$
- (ii)  $\mathbb{E}\{\mathbf{n}\} = 0$ ,  $\mathbb{E}\{\mathbf{n}\mathbf{n}^*\} = \sigma^2 \mathbf{I}$ ,  $\mathbb{E}\{\mathbf{n}\mathbf{n}^T\} = 0$  (spatial whiteness)
- (iii)  $\mathbf{R}_\gamma$  is non-singular (positive definiteness)

It is violation of (iii) that causes the MUSIC algorithm to completely fail. The latter is indeed the case when ranging with CSI in indoor environment due to the complete coherence between source vectors  $\gamma$  obtained for each new snapshot. Note that different snapshots are needed to calculate the empirical covariance matrix  $\hat{\mathbf{R}}_{\text{csi}} = 1/N_p \sum_{j_p=1}^{N_p} \text{csi}(j_p) \text{csi}(j_p)^H$  as  $\mathbf{R}_{\text{csi}}$  is never given in practice. Provided that time-domain averaging is ineffective, we perform averaging in other domains as discussed next.

### B. Spectral Smoothing

Since  $N_{\text{sc}} \gg N_{\text{mp}}$  and CSI are obtained by uniform sampling of CFR in the frequency domain, they possess invariant structure. The latter property means that the CSI vector can be partitioned into  $N_b$  spectral partitions of length  $N'_{\text{sc}} (> N_{\text{mp}})$  to perform averaging across those partitions by treating them as time samples. The idea behind spectral smoothing can be explained with an example; when  $N_b = 2$ , (19) is written as

$$\begin{bmatrix} \check{\text{csi}}_1 \\ \check{\text{csi}}_2 \end{bmatrix} = \begin{bmatrix} \mathbf{A}_1 \\ \mathbf{A}_2 \end{bmatrix} \cdot \gamma + \mathbf{n} \quad (22)$$

where,  $\check{\text{csi}}_1 = \check{\text{csi}}^{(1:N_{\text{sc}}/2)}$ ,  $\check{\text{csi}}_2 = \check{\text{csi}}^{(N_{\text{sc}}/2+1:N_{\text{sc}})}$ ,  $\mathbf{A}_1 = \mathbf{A}_{(1:N_{\text{sc}}/2, 1:N_{\text{mp}})}$ , and  $\mathbf{A}_2 = \mathbf{A}_{(N_{\text{sc}}/2+1:N_{\text{sc}}, 1:N_{\text{mp}})}$ . Now, given the definition of  $\mathbf{a}(\tau)$  in (20),  $\mathbf{A}_1 = \mathbf{A}_2 \cdot \mathbf{M}$  where  $\mathbf{M} = \text{diag}(z_1^{N_{\text{sc}}/2} \cdots z_{N_{\text{mp}}}^{N_{\text{sc}}/2})$ ,  $z_{j_{\text{mp}}} = \exp(-2\pi i \Delta f \tau_{j_{\text{mp}}})$ .

With this property, a hardened covariance matrix can be obtained by averaging individual sub-array's covariance matrices as  $\mathbf{R}_{\text{ss}} = 0.5(\mathbf{R}_{\check{\text{csi}}_1} + \mathbf{R}_{\check{\text{csi}}_2}) = \mathbf{A}_1 \mathbf{R}'_\gamma \mathbf{A}_1^H$  where  $\mathbf{R}'_\gamma = 0.5(\gamma\gamma^H + \mathbf{M}\gamma\gamma^H\mathbf{M}^H)$  has an improved rank, thus closer to the true source covariance matrix. In the general case, covariance hardening can be achieved if  $N_b \geq N_{\text{mp}}$  [35] through:

$$\mathbf{R}_{\text{ss}} = \frac{1}{N_b} \sum_{j_b=1}^{N_{\text{sc}} - N'_{\text{sc}} + 1} \mathbf{R}_{\text{csi}_{j_b}}^{(j_b:j_b+N'_{\text{sc}}-1, j_b:j_b+N'_{\text{sc}}-1)} \quad (23)$$

s.t.  $(j_b + N'_{\text{sc}} - 1 \leq N_{\text{sc}}/2$  or  $j_b \geq N_{\text{sc}}/2 + 1)$

where the constraints above are to ascertain that no sub-array contains  $k = 0$  subcarrier. This is an important consideration as no information is sent on  $k = 0$  (due to large DC current) causing  $\text{csi}^{(k=-1)}$  and  $\text{csi}^{(k=1)}$  to be  $2\Delta f$  apart instead of  $\Delta f$  (as is the case for other neighbouring subcarriers). Not paying attention to this when performing spectral smoothing adds to the estimation error.

Since the averaged covariance matrix has the exact structure as the original covariance matrix, MUSIC can be applied to obtain ToF estimates. This advantage came at the cost of reducing the effective length of the CSI vector ( $N_{\text{sc}} \rightarrow N'_{\text{sc}}$ ) and results in a tradeoff between resolution and stability of MUSIC solution.

### C. Forward-Backward Smoothing

The invariant structure of the CSI signal model can be used not only to smooth over the forward covariance submatrices but also the backward ones [36]. Mathematically, this operation is equivalent to

$$\mathbf{R}_{\text{csi}}^{\text{FW/BW}} = \mathbf{R}_{\text{csi}}^{\text{FW}} + \underbrace{\mathbf{J} \mathbf{R}_{\text{csi}}^{\text{FW}*} \mathbf{J}}_{\mathbf{R}_{\text{csi}}^{\text{BW}}} \quad (24)$$

where  $\mathbf{J}$  is an  $N_{\text{sc}} \times N_{\text{sc}}$  exchange matrix with ones only on the anti-diagonal and  $\mathbf{R}_{\text{csi}}^{\text{FW}}$  is the forward covariance matrix which is given by (23). Using forward-backward smoothing, the empirical covariance matrix in (24) gets closer to the true CSI covariance matrix improving the accuracy of the MUSIC estimator that heavily relies on the knowledge of this matrix.

### D. Decision Fusion

As detailed before, CSI is a matrix characterizing the channels between each transmit antenna  $j_{\text{tx}}$  and receive antenna  $j_{\text{rx}}$ . Provided that transmit antennas (and receive antennas) are spatially sufficiently separated, CSI provides us with  $j_{\text{rx}} \times j_{\text{tx}}$  independent sub-channels which can be used to obtain independent estimates of range. By fusing these decisions at last, one expects a more accurate final range estimate. One should note that CSI over different sub-channels cannot be stacked up to form a single covariance matrix (named fusion over raw measurement), as the steering matrix  $\mathbf{A}$  in (19) is different for different transmit-receive sub-channels. Fig. 9 illustrates pseudo-spectrums calculated from measurement in corridors of University of Toronto (UofT) where transmitter and receiver were 45m apart.

Different pseudo-spectrums peak at different ranges ( $\hat{d}_{j_{\text{rx}}, j_{\text{tx}}}$ ) for two reasons: (i) some  $(j_{\text{rx}}, j_{\text{tx}})$  sub-channels

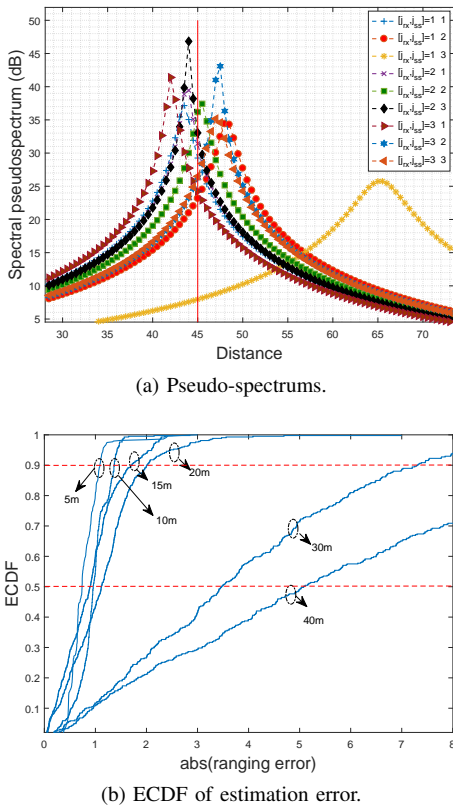


Fig. 9: (left) Pseudo-spectrums derived for real-world measurements for different  $(j_{rx}, j_{tx})$  pairs when transmitter-receiver are 45m apart (red vertical line). (right) ECDF of estimation error when transmitter and receiver are 5, 10, 15, 20, 30, 40m apart.

are weaker thus giving rise to larger random shifts in their corresponding pseudo-spectrums (ii) multipath fading impacts sub-channels differently.

How do we combine  $\hat{d}_{j_{rx}, j_{tx}}$ s to get a more accurate range estimate? Simply averaging them yields inaccurate range estimates. The solution we propose is to obtain all sub-channel pseudo-spectrums for all post-processed CSI packets and:

- 1) identify those  $\hat{d}_{j_{rx}, j_{tx}}$  that fluctuate the most (in time). Apply any outlier rejection method to remove that sub-channel from decision-making process. For example, that peak is  $\hat{d}_{1,3}$  in Fig. 9.
- 2) weight the remaining pseudo-spectrum peaks with their corresponding averaged (w.r.t  $k$ ) CSI magnitudes, i.e.  $w_{j_{rx}, j_{tx}} = 1/N_{sc} \sum_k |\text{csi}_{j_{rx}, j_{tx}}^{(k)}|$ . The logic is that a weaker sub-channel is more impacted by the noise components when CSI matrix is being estimated by the receiver through simple zero-forcing (ZF) or minimum-mean-square (MMSE) algorithms. Since the weakness/strength of a sub-channel is manifested in the total energy spread across frequency components, the above weighting put more emphasis on the stronger sub-channels that are less impacted by estimation noise.

## VI. EXPERIMENTAL RESULTS

We performed extensive experiments using IEEE802.11n Atheros 93xx chipset in two environments: (i) Anechoic

chambers (multipath-free) in Fig. 7c (ii) corridors (multipath) in Fig. 7a and Fig. 7b. We collected a few thousands CSI, post-processed them using the techniques introduced in Section IV, formed the spatially-smoothed covariance matrix, applied spectral MUSIC algorithm, fused final decisions, and obtained one final estimate. We repeated this experiment for all the collected CSI set. Fig. 9b plots the empirical cumulative distribution function (ECDF) of the estimation error: According to this plot, the median accuracy of 60, 80, 90, 115, 140, 350, and 500cm is achieved when transmitter-receiver are 5, 10, 15, 20, 25, 30, and 40m apart respectively. The 90th percentile accuracy is about 1m (at 5m) and 1.7m (at 20m). Note that at 40m distance, the received power is about -100dB which is only a few decibels higher than the noise floor. One should note that using raw CSI yields range estimates that are off by several tens of meters. Provided that the range estimation error is even larger than the maximum WiFi coverage, which is about 20m in current MIMO-OFDM systems, there is truly no value in comparing calibrated and uncalibrated range estimates. Moreover, since our work is the first to exploit the CSI phase to obtain range estimates, it was impossible to benchmark our results with the previous studies that are based on angle of arrival (AoA) estimation.

Contrary to the claims made in the literature [2], [5], our results suggest that sub-meter ranging accuracy is possible using CSI obtainable from commodity WiFi. There are several observations that were made in the course of the project which are worth mentioning:

- With 20MHz of spectrum available for WiFi signals, one shall not expect to resolve multipath components with MUSIC or with any high-resolution estimation algorithm. This is evident from Fig. 9a for 9 sub-channels of a highly fading propagation environment.
- Due to the limited resolvability power achievable with 20MHz CSI, spectral smoothing with only a handful of partitions is able to sufficiently harden the covariance matrix and recover the only expected peak.
- When SNR is low (which happens at longer distances), receiver chooses to advance more than one symbol to make sure any mistake in detecting the symbol boundary estimation (using cross-correlation of HT-LTF sequence with the received header) wouldn't cause erroneous outcomes.
- In situations when  $d^{\text{truth}} < \epsilon^{\text{pre}}$ , the pseudo-spectrum has a (one-sided) peak at  $d = 0$  which signifies the existence of a hidden (two-sided) peak at negative distances. When that's the case, the RSSI-assisted approach won't work as the knowledge of the hypothesis set  $\mathcal{D} = \{\hat{d}, \hat{d} + 15m, \hat{d} + 30m, \dots\}$ , delineated in subsection IV-D, hinges on the knowledge of the two-sided  $\hat{d}$ . To cope with this situation, after post-processing CSI, one will have to deliberately rotate (leftwise) the CSI phase (before forming the pseudo-spectrum) by a few samples to recover peaks at negative distances (due to the existence of pre-advancement error) and de-rotate those peaks for the *same number of samples* to cancel out what was artificially added. Then RSSI-based hypothesis

testing is applied to find out the true range estimate.

- This work does not consider tracking of user's range parameter through combining motion information (obtainable using prevalent inertial measurement units (IMU)) with instantaneously obtained range estimates. Therefore, it is believed that such fusion of information (e.g. using *Kalman* filter) would yield more stable and accurate results.

## VII. CONCLUSION

The availability of channel-state information (CSI) from WiFi chipsets has made indoor positioning a reality. Leveraging the CSI, several recent studies have achieved decimeter accuracy through angle-of-arrival (AoA) estimation or wide-band ranging. When it comes down to implementation, the CSI-based localization with time-of-flight (ToF) measurement from only a single channel (20 MHz of spectrum) has either not been pursued or led to inconsistent results. With the knowledge of fundamental limits of ranging and its reliance on the availability of bandwidth, the critical question has always been “whether sub-meter ranging is possible with such limited bandwidth”. This paper aims to answer this question. We dissect different deterministic and random phenomena happening in the transmitter and receiver hardware and establish the right model for CSI. We propose techniques to eliminate random phases introduced by the insufficiency of synchronization between transmitter and receiver. Our range estimates using the MUSIC algorithm show that median accuracy of 0.6m (1.15m) is achievable in highly multipath line-of-sight environment where transmitter and receiver are 5m (20m) apart. Moreover, with 90th percentile accuracy of 1.1m (2m) in 5m (20m), we can claim that the proposed system is robust.

## REFERENCES

- [1] D. Ferris, D. Fox, and N. Lawrence, “WiFi-SLAM using Gaussian process latent variable models,” in *Proc. 20th Intl. Joint Conf. Artificial Intel. (IJCAI'07)*, Jan. 2007, pp. 2480–2485.
- [2] M. Kotaru, K. Joshi, D. Bharadia, and S. Katti, “SpotFi: Decimeter level localization using WiFi,” in *ACM Special Interest Group Data Commun. (SIGCOMM'15)*, vol. 45, no. 4, June 2015, pp. 269–282.
- [3] J. Xiong and K. Jamieson, “Arraytrack: a fine-grained indoor location system,” in *USENIX Symp. Networked Syst. Des. Implementation (NSDI'13)*, Apr. 2013, pp. 71–84.
- [4] S. Sen, J. Lee, K. Kim, and P. Congdon, “Avoiding multipath to revive inbuilding WiFi localization,” in *ACM Int. Conf. Mobile Syst., Appl., Services (MobiSys'13)*, Jun. 2013, pp. 249–262.
- [5] D. Vasisht, S. Kumar, and D. Katabi, “Decimeter-level localization with a single WiFi access point,” in *USENIX Symp. Networked Syst. Des. Implementation (NSDI'16)*, Mar. 2016, pp. 165–178.
- [6] A. Mariakakis, S. Sen, J. Lee, and K. Kim, “SAIL: Single access point-based indoor localization,” in *ACM Int. Conf. Mobile Syst., Appl., Services (MobiSys'14)*, Jun. 2014, pp. 315–328.
- [7] C. Yang and H. Shao, “WiFi-based indoor positioning,” *IEEE Commun. Mag.*, vol. 53, no. 3, pp. 150–157, Mar. 2015.
- [8] K. Chintalapudi, A. P. Iyer, and V. N. Padmanabhan, “Indoor localization without the pain,” in *Proc. 16th Annu. Intl. Conf. Mobile Computing Networking (MobiCom'10)*, Sep. 2010, pp. 173–184.
- [9] P. Bahl and V. N. Padmanabhan, “RADAR: an in-building RF-based user location and tracking system,” in *IEEE Int. Conf. Comput. Commun. (INFOCOM)*, vol. 2, Mar. 2000, pp. 775–784.
- [10] M. Youssef and A. Agrawala, “The Horus WLAN location determination system,” in *Proc. 3rd Int. Conf. Mobile Syst., Appl., Services (MobiSys'05)*, Jun. 2005, pp. 205–218.
- [11] M. Azizyan, I. Constandache, and R. Choudhury, “Surroundsense: Mobile phone localization via ambience fingerprinting,” in *Proc. 15th Annu. Intl. Conf. Mobile Computing Networking (MobiCom'09)*, Sep. 2009, pp. 261–272.
- [12] J. Xiao, Z. Zhou, Y. Yi, and L. Ni, “A survey on wireless indoor localization from the device perspective,” *ACM Computing Surveys (CSUR)*, vol. 49, no. 2, pp. 1–25, Nov. 2016.
- [13] Z. Yang, Z. Zhou, and Y. Liu, “From RSSI to CSI: Indoor localization via channel response,” *ACM Computing Surveys (CSUR)*, vol. 46, no. 2, pp. 1–25, Nov. 2013.
- [14] S. Gezici, Z. Tian, G. V. Giannakis, H. Kobayashi, A. Molisch, H. V. Poor, and Z. Sahinoglu, “Localization via ultra-wideband radios: A look at positioning aspects for future sensor networks,” *IEEE Signal Process. Mag.*, vol. 22, no. 4, pp. 70–84, Jul. 2005.
- [15] S. Sorour, Y. Lostonlen, S. Valaee, and K. Majeed, “Joint indoor localization and radio map construction with limited deployment load,” *IEEE Transactions on Mobile Computing*, vol. 14, no. 5, pp. 1031–1043, May 2015.
- [16] C. Feng, W. Au, S. Valaee, and Z. Tan, “Received-signal-strength-based indoor positioning using compressive sensing,” *IEEE Trans. Mobile Comput.*, vol. 11, no. 12, pp. 1983–1993, Dec. 2012.
- [17] D. Halperin, W. Hu, A. Sheth, and D. Wetherall, “Tool release: Gathering 802.11n traces with channel state information,” *ACM SIGCOMM Comput. Commun. Review*, vol. 41, no. 1, pp. 53–53, Jan. 2011.
- [18] Y. Xie, Z. Li, and M. Li, “Precise power delay profiling with commodity WiFi,” in *Proc. 21st Annu. Intl. Conf. Mobile Computing Networking (MobiCom'15)*, Sep. 2015, pp. 53–64.
- [19] M. Rahman, N. Tadayon, S. Han, and S. Valaee, “LocHunt: Angle-of-arrival based location estimation in harsh multipath environment,” in *2018 IEEE Global Commun. Conf. (Globecom)*, Dec. 2018, accepted for publication.
- [20] E. Perahia and R. Stacey, *Next generation wireless LANs: 802.11n and 802.11ac*, 2nd ed. Cambridge: Cambridge University Press, 2013.
- [21] R. V. Nee, V. K. Jones, G. Awater, A. V. Zelst, J. Gardner, and G. Steele, “The 802.11n MIMO-OFDM standard for wireless LAN and beyond,” *Wireless Personal Commun.*, vol. 37, no. 3–4, pp. 445–453, June 2006.
- [22] “IEEE standard for information technology—local and metropolitan area networks—specific requirements—part 11: Wireless LAN medium access control (MAC) and physical layer (PHY) specifications amendment 5: Enhancements for higher throughput,” *IEEE Standard 802.11n*, pp. 1–565, Oct. 2009.
- [23] K. Wu, J. Xiao, Y. Yi, D. Chen, X. Luo, and L. Ni, “CSI-based indoor localization,” *IEEE Trans. Parallel Distrib. Syst.*, vol. 24, no. 7, pp. 1300–1309, Jul. 2013.
- [24] M. Speth, S. A. Fechtel, G. Fock, and H. Meyr, “Optimum receiver design for wireless broad-band systems using OFDM—Part I,” *IEEE Trans. Commun.*, vol. 47, no. 11, pp. 1668–1677, Nov. 1999.
- [25] H. Zhu, Y. Zhuo, Q. Liu, and S. Chang, “ $\pi$ -Splicer: Perceiving accurate CSI phases with commodity WiFi devices,” *IEEE Trans. Mobile Comput.*, pp. 1–9, May 2017.
- [26] Z. Zhou, Z. Yang, C. Wu, W. Sun, and Y. Liu, “LiFi: Line-of-sight identification with WiFi,” in *IEEE Int. Conf. Computer Communications (INFOCOM)*, Apr. 2014, pp. 2688–2696.
- [27] T. M. Schmidl and D. C. Cox, “Robust frequency and timing synchronization for OFDM,” *IEEE Trans. Commun.*, vol. 45, no. 12, pp. 1613–1621, Dec. 1997.
- [28] E. A. Ansari and N. Rajatheva, “Exact SER analysis of OSTBC MIMO-OFDM systems over uncorrelated Nakagami-m fading channels,” in *IEEE 13th Int. Multitopic Conf. (INMIC '09)*, Dec. 2009, pp. 1–6.
- [29] P. C. Weeraddana, N. Rajatheva, and H. Minn, “Probability of error analysis of BPSK OFDM systems with random residual frequency offset,” *IEEE Trans. Commun.*, vol. 57, no. 1, pp. 106–116, Jan. 2009.
- [30] S. Sen, B. Radunovic, R. R. Choudhury, and T. Minka, “You are facing the Mona Lisa: Spot localization using PHY layer information,” in *ACM Int. Conf. Mobile Syst., Appl., Services (MobiSys'12)*, Jun. 2012, pp. 183–196.
- [31] X. Xiong, K. Sundaresan, and K. Jamieson, “ToneTrack: Leveraging frequency-agile radios for time-based indoor wireless localization,” in *Proc. 21st Annu. Intl. Conf. Mobile Computing Networking (MobiCom'15)*, Sep. 2015, pp. 537–549.
- [32] X. Li and K. Pahlavan, “Super-resolution TOA estimation with diversity for indoor geolocation,” *IEEE Trans. Wireless Commun.*, vol. 3, no. 1, pp. 224–234, Jan. 2004.
- [33] R. Schmidt, “Multiple emitter location and signal parameter estimation,” *IEEE Trans. Antennas Propag.*, vol. 34, no. 3, pp. 276–280, Mar. 1986.

- [34] P. Stoica and A. Nehorai, "MUSIC, maximum likelihood, and Cramer-Rao bound," *IEEE Trans. Acoust., Speech, Signal Process.*, vol. 37, no. 5, pp. 720–741, May 1989.
- [35] T. Shan, M. Wax, and T. Kailath, "On spatial smoothing for direction-of-arrival estimation of coherent signals," *IEEE Trans. Acoust., Speech, Signal Process.*, vol. 33, no. 4, pp. 806–811, Aug. 1985.
- [36] S. Pillai and B. H. Kwon, "Forward/backward spatial smoothing techniques for coherent signal identification," *IEEE Trans. Acoust., Speech, Signal Process.*, vol. 37, no. 1, pp. 8–15, Jan. 1989.